Journal of Environmental Chemical Engineering 10 (2022) 108567

Contents lists available at ScienceDirect

Journal of Environmental Chemical Engineering

journal homepage: www.elsevier.com/locate/jece

Copper ion-exchanged zeolite X from fly ash as an efficient adsorbent of phosphate ions from aqueous solutions

Jakub Mokrzycki [a,*], Monika Fedyna [b], Mateusz Marzec [c], Justyna Szerement [a], Rafał Panek [d], Agnieszka Klimek [a], Tomasz Bajda [a], Monika Mierzwa-Hersztek [a,e]

[a] Faculty of Geology, Geophysics and Environmental Protection, AGH University of Science and Technology, Mickiewicza 30 Av., 30-059 Cracow, Poland
[b] Faculty of Chemistry, Jagiellonian University, Gronostajowa 2, 30-387 Cracow, Poland
[c] Academic Centre for Materials and Nanotechnology, AGH University of Science and Technology, Mickiewicza 30 Av., 30-059 Cracow, Poland
[d] Department of Geotechnical Engineering, Civil Engineering and Architecture Faculty, Lublin University of Technology, Nadbystrzycka 40, 20-618 Lublin, Poland
[e] Department of Agricultural and Environmental Chemistry, University of Agriculture in Krakow, Mickiewicza 21 Av., 31-120 Cracow, Poland

ARTICLE INFO

Editor: Teik Thye Lim

Keywords:
Fly-ash-derived zeolite
Ion-exchange
Phosphate ions adsorption
Copper

ABSTRACT

Zeolite X derived from fly ash was modified with $Cu(NO_3)_2 \bullet 3\ H_2O$ solutions of various initial concentrations (0.01, 0.05, 0.10, 0.15, and 0.20 M). The obtained materials were investigated by means of XRD, XRF, N_2 adsorption-desorption, and pHpzc. The concentration of $Cu(NO_3)_2 \bullet 3\ H_2O$ significantly affected both the textural and chemical surface properties of the obtained zeolites. The materials were subjected to a series of adsorption experiments to remove phosphate ions from aqueous solutions. The highest adsorption capacity was obtained for zeolite X modified with 0.05 M $Cu(NO_3)_2 \bullet 3\ H_2O$ solution, and the obtained adsorption capacity was 87.7 mg (PO_4^{3-}) g^{-1}. The adsorption mechanism was investigated by means of XPS analysis and correlated with the assumptions of kinetic adsorption models. The interaction between phosphate ions and Cu species on the zeolite surface was found to be the guiding mechanism of adsorption. Additional mechanisms, including precipitation as calcium phosphate and electrostatic attraction, should also be taken into account. A single-point adsorption of phosphate ions was also studied to evaluate the effects of adsorbent dose (1, 2, and 3 g L^{-1}) and adsorption temperature (18, 25 and 40 °C). Increased adsorbent dose resulted in a significantly greater removal of phosphate ions for zeolite Cu0.05X (up to 65.4%). The temperature of 25 °C was found to be the most suitable for conducting adsorption of phosphate ions. Leaching test was performed in water to investigate the risk of applying the investigated zeolites in aqueous solutions as potential adsorbents.

1. Introduction

Phosphorus is an essential element for plant growth, supplied to the soil by fertilizers. Unfortunately, the increased use of fertilizers, required by agricultural intensification, has greatly accelerated the leakage of phosphorous from soil to water, resulting in an endemic global problem called eutrophication [1]. Increased concentration of phosphorus in water can lead to excessive growth of algae and as consequence to the reduction in the dissolved oxygen causing ecosystem damage [2]. Sources of phosphorous release to the environment to the greatest extent include agriculture, urban run-off, animal wastes, human sewage, industry and detergents [3]. According to Polish standards, the concentration of phosphorus in lakes should not exceed 0.03 mg L^{-1} [4,5]. For instance, in the United Kingdom, the level of phosphorous in potable water should be below 1 mg L^{-1}, and similar limitations can be found in other countries [6]. Referring to the World Health Organization (WHO), the permissible limit of phosphorus in water is 10 mg L^{-1}. Phosphorus is present in water in ionic forms. The form of phosphate ions in water is closely related to the pH. For pH< 2, the most dominant form is H_3PO_4, for pH from about 3–7 $H_2PO_4^-$, from 7 to about 11 HPO_4^{2-}, and above 12 PO_4^{3-}. When addressing the dissociation constant (pKa) of H_3PO_4, the formation of PO_4^{3-} ions is less dominant in wastewaters than the above-mentioned monovalent and divalent forms. Therefore, $H_2PO_4^-$ and HPO_4^{2-} ions predominate [7].

Phosphorus is a non-renewable resource and is crucial for the development of life and agricultural production. According to many reports, the global phosphate reserves will be depleted within the next 50–100 years. Taking into account the scarcity of that resource in the

* Corresponding author.
E-mail address: jmokrzycki@agh.edu.pl (J. Mokrzycki).

https://doi.org/10.1016/j.jece.2022.108567
Received 6 July 2022; Received in revised form 12 August 2022; Accepted 7 September 2022
Available online 12 September 2022

future, the development of cost-effective methods to recover phosphorous, *i.e.* from waters, becomes necessary for both sustainable development and environmental protection [8].

Many studies have been conducted to remove phosphate ions from aqueous solutions/wastewaters, *i.e.* biological, chemical, and physical treatments. However, well-known processes such as biological treatment, precipitation, or crystallization as struvite require high phosphate concentrations. Biological treatment requires strict temperature and pH conditions to allow the microorganisms activity. On the other hand, chemical precipitation method, despite high efficiency and simple operation can cause sludge disposal problems [9]. Therefore, other methods should be used to overcome that obstacle of low phosphate concentration. As a result, much attention is now paid to the removal of phosphate ions *via* adsorption [10]. The most important advantages of adsorption are: relatively low processing and energy costs, selectivity, fast rates, operation at low concentrations, and adsorbent recovery [11]. Adsorbents including microporous materials, *i.e.* zeolites (A, X, P1, ZSM-5) [12–16] or MOFs [17], and mesoporous materials, *i.e.* MCM-41 [18] or SBA-15 [19,20], proved to be highly effective as phosphate ions adsorbents. Nevertheless, sufficient performance of those materials in the adsorption of phosphate ions was possible only after certain chemical modifications to increase their affinity for phosphate ions. Among the above materials, zeolites have received the most attention in the adsorption of phosphate ions. Although zeolites are a group of materials characterized by high cation exchange properties, sufficient specific surface area (S_{BET}), ordered and stable microporous structure, they have also been recognized as effective materials for capturing phosphate ions as oxoanionic species [21,22]. Zeolites themselves possesses rather weak adsorption properties, thus they modification is required. Transition metal cations can be easily doped into the framework to optimize the desired performance of specific zeolite frameworks [23]. Wang et al. reported the adsorption of Cu^{2+} using synthetic zeolites A and X. The ion exchange properties towards heavy metals strictly depended on the amount of exchangeable Na^{+} ions which intensively corelates with the molar Si/Al ratio of the zeolite [24]. The most recent methods to increase the adsorption capacity of zeolites towards phosphate ions involve the incorporation of lanthanum [25], iron [26], hydrated aluminum oxide [27], titanium oxide [28], and geopolymers [29]. Another important possibility of using zeolites as phosphate ions adsorbents is their production from fly ash, which has been widely investigated in the literature [21,30,31]. Fly ash is one of the emerging industrial solid waste generated by coal-fired power plants and thermal power plants. Due to inadequate utilization technologies and occupation of large areas while landfilling, fly ash has become an environmental concern. The most common methods of its disposal, which accounts for about 60–70% are: application of fly ash in civil engineering as an additive to cements, production of ceramics, and stabilization of wastes. Similar chemical composition of fly ash and zeolites (SiO_2 and Al_2O_3) enables fly ash application as raw material for zeolite synthesis, which has become an alternative route for fly ash recycling [31,32]. The most common method of zeolite synthesis using fly ash is the hydrothermal process. Briefly, fly ash and an alkaline agent (NaOH, KOH) are mixed under specific conditions (time, temperature, solution pH, component ratio) to obtain the desired zeolite type, often a single and high crystalline phase [24].

The aims of the present study were to: (*i*) obtain new and highly efficient adsorbents of phosphate ions *via* simple one-step ion exchange of fly-ash-derived zeolite X; (*ii*) investigate the effect of copper nitrate ($Cu(NO_3)_2 \bullet 3\ H_2O$) solution on adsorption capacity; (*iii*) investigate the adsorption statics in a wide range of phosphate ions concentrations from 10 to 200 mg L^{-1} and compare the obtained results with Langmuir and Freundlich adsorption isotherms; (*iv*) investigate the adsorption process and its mechanisms using various mathematical models: pseudo-first order, pseudo-second order, Bangham, Elovich, Weber-Morris; and by means of the instrumental method (X-ray photoelectron spectroscopy); (*v*) investigate the effect of operating conditions, *i.e.* adsorbent dose and adsorption temperature, on phosphate ions adsorption; (*vi*) conduct a leaching test in water aiming to investigate the potential risk of applying adsorbents in aqueous media. To the best of our knowledge, this is the first study devoted to the modification of zeolite with copper salt solution to investigate the adsorption of phosphate ions.

2. Materials and methods

2.1. Zeolite NaX synthesis and ion exchange with Cu^{2+} ions

The main component for the synthesis of ultrapure zeolite NaX was liquid waste from the production of zeolite from fly ash on a semi-technical line [33]. That waste was an alkaline solution rich in silicon, which allowed for effective use in the described synthesis. The details of synthesis have recently been described in the study by Panek et al. [34] and in the Supplementary Information.

To prepare copper-exchanged zeolites, 1 g of ultrapure zeolite NaX was weighed into a 250 mL beaker. Then 100 mL of $Cu(NO_3)_2 \bullet 3\ H_2O$ (Sigma-Aldrich) solution was added. The initial concentrations of $Cu(NO_3)_2 \bullet 3\ H_2O$ solutions were: 0.01, 0.05, 0.10, 0.15, and 0.20 M. The mixture was then stirred using a magnetic stirrer (500 rpm) for 24 h at 25 °C. After ion exchange, the zeolite was washed several times with distilled water and air-dried overnight. The zeolite was then dried in an oven at 110 °C for 12 h. The obtained materials were denoted as Cu0.01X, Cu0.05X, Cu0.10X, Cu0.15X, and Cu0.20X.

2.2. Characterization of materials

2.2.1. X-ray diffraction (XRD)

The XRD measurement was performed using an X'pert PROMPD diffractometer with a PW3050/60 goniometer and a Rigaku SmartLab diffractometer (Tokyo, Japan). Both were equipped with a CuKα radiation and graphite monochromator. The range of 2θ varied from 2° to 50° in 0.05° increments.

2.2.2. Nitrogen adsorption-desorption at 77 K

The textural parameters of zeolite NaX and its Cu-modified forms were determined by means of a low-temperature nitrogen adsorption/desorption isotherm. All analyzes were conducted on an ASAP 2020 instrument (Micromeritics, Norcross, GA, USA). The analysis details are given in the Supplementary Information.

2.2.3. X-ray fluorescence (XRF)

The chemical composition of zeolite samples was determined by the X-ray fluorescence (XRF) technique using an ARL QUANT'X spectrometer (Thermo Scientific, Waltham, MA, USA) with a rhodium anode (4–50 kV in 1 kV increments) and beryllium windows. A 1 mm beam and a 3.5 mm Si(Li) drifted crystal detector with Peltier cooling (~185 K) were used for all measurements. Quantitative analysis of elements in zeolite samples was preformed using UniQuant software and metallic calibration standards.

2.2.4. pH point of zero charge (pHpzc)

The pHpzc value was determined according to the method described by Kragović et al. [35]. Briefly, sodium nitrate ($NaNO_3$) solution with an initial concentration of 0.01 M was used as a background electrolyte. The initial pH (pH_{in}) of the background electrolyte solution was adjusted to 5.5; 6.5; 7.5; 8.0; 8.5; 9.0; and 10.0 using 0.1 M NaOH (Avantor) and 0.1 M HNO_3 (Avantor) solutions and measured using an ELMETRON CX-502 pH meter equipped with a glass electrode (Elmetron). Exactly 50 mg of zeolite was weighed into a 50 mL plastic flask and 25 mL of the electrolyte solution was added. The flasks were then placed in a laboratory shaker and vigorously stirred for 24 h at room temperature. The samples were then centrifuged at 4500 rpm for 5 min and the final pH values of the obtained supernatant were measured. The pHpzc value was determined by plotting the difference between the final and the initial

pH (ΔpH) against pH_{in}. The experiments were performed in duplicate.

2.2.5. X-ray photoelectron spectroscopy (XPS)

XPS analyzes were carried out in a PHI VersaProbeII Scanning XPS system using monochromatic Al Kα (1486.6 eV) X-rays focused to a 100 μm spot and scanned over the area of 400 μm x 400 μm. The photoelectron take-off angle was 45° and the pass energy in the analyzer was set to 117.50 eV (0.5 eV increments) for survey scans and to 46.95 eV (0.1 eV increments) to obtain high energy resolution spectra for the C 1 s, O 1 s, P 2p, Si 2p, Ca 2p, K 2p, Al 2p, Na 1 s, and Cu 2p regions. The analysis details are given in the Supplementary Information.

2.3. Static adsorption of phosphate ions

The experimental conditions were selected based on the previous study [21]. Static adsorption experiments of phosphate ions were performed in 100 mL Erlenmeyer flasks. The concentrations of phosphate ions varied from 10 to 200 mg (PO_4^{3-}) L^{-1}. The solutions were prepared prior to the adsorption experiments by dissolving KH_2PO_4 (Sigma-Aldrich) in distilled water. The pH of the solutions was adjusted to 5.00 ± 0.10 using 0.05 M solutions of HNO_3 (Avantor) or NaOH (Avantor). Exactly 50 mg of zeolite (dried overnight at 105 °C prior to the experiment) was weighed and mixed with 50 mL of KH_2PO_4 solution to maintain a zeolite to solution ratio of 1 g L^{-1}. The samples were mixed using an orbital shaker (GFL 3015, SciQuip, UK) for 24 h. After that time, the zeolite-solution system reached equilibrium concentration. Then the solutions were centrifuged, and the concentration of phosphate ions was measured using a spectrophotometer (HITACHI U-5100, Hitachi High-Tech Science Corporation, Tokyo, Japan) at a wavelength of 700 nm. The experiments were performed in triplicate. The adsorption capacity (q_{eq}), which represents the amount of phosphate ions adsorbed by the sorbent, was calculated from the equation given in Table S1.

The obtained results were correlated with Langmuir and Freundlich models. The Freundlich sorption model assumes multilayer adsorption on a heterogeneous adsorbent surface [36]. The Langmuir sorption model, in contrast to the Freundlich model, assumes that the sorbent surface is homogenous and a monolayer of adsorbate is formed [37]. Additionally, the Langmuir model can be used to calculate a dimensionless parameter (R_L), which indicates whether the sorption is favorable or not (R_L>1 – unfavorable, R_L=1 – linear adsorption, 1 >R_L>0 – favorable adsorption, R_L=0 – irreversible adsorption) [38,39]. The linear forms of the models and the formulas for calculating the adsorption capacity (q_{eq}) and the R_L parameter are presented in Table S1.

2.4. Kinetic adsorption of phosphate ions

A series of kinetic studies were conducted using NaX and Cu0.05X to investigate the possible mechanisms of adsorption. The experimental conditions were selected based on the previous study [21]. Adsorption kinetics experiments were performed in 250 mL beakers by adding 100 mL of phosphate solution with an initial concentration of 80 mg (PO_4^{3-}) L^{-1} and an initial pH of 5.00 ± 0.10, to 100 mg of zeolite sample (dried overnight at 105 °C prior to the experiment). The zeolite solution was stirred using a magnetic stirrer, and then samples were collected at specific time intervals (total of 24 h at 25 °C) for phosphate ions concentration analysis by the method described in Section 2.4. Samples were collected from the same beaker throughout the experiment using membrane filters (0.22 μm) to separate the zeolite from the solution. The experiments were performed in triplicate. The obtained experimental results were correlated with the adsorption kinetic models given in Table S2.

2.5. Effects of adsorbent dose and adsorption temperature on phosphate ions adsorption

Zeolites NaX and Cu0.05X were selected for the single-point adsorption study. The effect of adsorbent dose was studied under static conditions at room temperature. The selected doses were 1, 2, and 3 g L^{-1}. The solution volume in each case was 50 mL of KH_2PO_4 with an initial concentration of 80 mg (PO_4^{3-}) L^{-1} and initial pH of 5.00 ± 0.10. The samples were mixed using an orbital shaker. The solutions were collected after 24 h and analyzed as described in Section 2.3. The experiments were carried out in triplicate.

The effect of temperature was studied under static conditions. Briefly, 50 mg of zeolite was mixed with 50 mL of KH_2PO_4 solution with an initial concentration of 80 mg (PO_4^{3-}) L^{-1} and an initial pH of 5.00 ± 0.10. The mixtures were placed in a magnetic stirrer equipped with a water bath. The experiment was performed at three different temperatures: 18 ± 1 °C, 25 ± 1 °C or 40 ± 1 °C in incubated flasks. The solutions were collected after 24 h and analyzed as described in Section 2.3. The experiments were carried out in triplicate.

2.6. Leaching test

The leaching test was performed for zeolites NaX and Cu0.05X, according to the following procedure. Briefly, 100 mg of zeolite was mixed with 100 mL of distilled water using a magnetic stirrer for 24 h at 25 °C. The solution samples were then separated from the mixture using membrane filters (0.22 μm) and measured using inductively coupled plasma optical emission spectrometry (ICP-OES, OPTIMA 7200DV, Perkin Elmer) to identify the solution composition according to ISO [40]. The experiments were carried out in duplicate.

3. Results and discussion

3.1. Materials characterization

3.1.1. X-ray diffraction (XRD)

The XRD patterns of the investigated materials are shown in Fig. 1. The different intensities of the peaks as compared to the parent NaX indicate the preferential deposition of Cu over various locations in zeolite [41]. It should be noted that the crystalline structure of FAU zeolite is retained after modification. However, some characteristic peaks of zeolite NaX decreased in intensity: 2θ 6.10, 10.00, 15.45, 23.30, 26.65, and 30.95° after ion exchange with Cu^{2+} ions. That phenomenon was also reported by Yao et al. [42] and Benaliouche et al. [43], where an increase in the concentration of Cu ions used for ion exchange resulted in a decrease in the intensities of zeolite NaX characteristic peaks. Hence, the structure of the fly-ash-derived zeolite NaX was

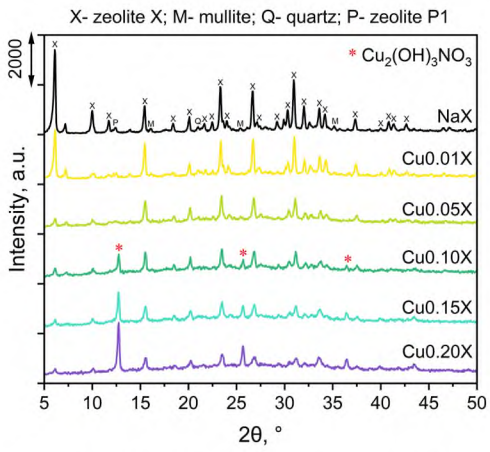

Fig. 1. XRD patterns of zeolite NaX and Cu ion-exchanged zeolite NaX.

affected during modification. The shift of some 2θ values after ion exchange at higher $Cu(NO_3)_2 \bullet 3\ H_2O$ solution concentrations (0.10 M and above) may result from the exchange of a small sodium cation by a larger copper ion [44]. Some characteristic peaks (2θ 12.4, 25.7, and 36.5°) appeared when the $Cu(NO_3)_2 \bullet 3\ H_2O$ concentration was 0.10 M and above. Their intensities increased with increasing solution concentration. According to the literature, those peaks are assigned to the complex compound $Cu_2(OH)_3NO_3$ [45]. Some small peaks identified as mullite (M), quartz (Q), and zeolite P1 (P), were also found and assigned in the XRD pattern [46].

3.1.2. N_2 adsorption-desorption at 77 K

The obtained materials were characterized by the N_2 adsorption-desorption method at 77 K to investigate the textural properties of zeolites. The results are presented in Fig. 2 and Table 1. As can be seen, increasing the concentration of $Cu(NO_3)_2 \bullet 3\ H_2O$ solution above 0.01 M used for ion exchanged caused a significant decrease in specific surface area (S_{BET}), total pore volume (V_t), and micropore volume (V_{mic}) of the obtained materials compared to the parent zeolite NaX. No significant decrease in micropore volume (V_{mic}) was observed for Cu0.10X, Cu0.15X, and Cu0.20X samples. All samples displayed type IVa isotherm curve according to the IUPAC characterization. The type IVa of isotherm curve is characterized by a rapid increase in N_2 monolayer adsorption at lower p/p_0 values. The shape of the curve results form the unrestricted mono- and multilayer adsorption up to high p/p_0 [47,48]. The hysteresis loop was present in all Cu-exchanged materials. Zeolites Cu0.01X, Cu0.10X, Cu0.15X, and Cu0.20X were characterized by the type H3 hysteresis loop, as classified by IUPAC, while Cu0.05X displayed the type H2/H3 [49,50]. The occurrence of characteristic H3 hysteresis loop is related to nonhomogeneous mesopores and/or micropores (bottle-shaped pores) generated during ion exchange. The impeded access of Cu^{2+} ions to the zeolite pores may cause distortion of the channels [51]. Some studies emphasized that during ion exchange two Na^+ ions are replaced by one Cu^{2+} ion [52]. As a result, the pores of zeolites become wider, as can be seen from the average pore diameter (D) and the decrease in micropore volume (V_{mic}) of the materials (Table 1). Furthermore, the XRD patterns (Fig. 1) proved that $Cu_2(OH)_3NO_3$ species are formed above $Cu(NO_3)_2 \bullet 3\ H_2O$ solution concentration of 0.10 M, which may cause pore blockage and/or mesopore formation. The high concentration of Cu^{2+} ions in the solution also significantly affected S_{BET}, which was nearly 7.6 times lower for Cu0.20X compared

Table 1
Textural properties of the investigated zeolites and their pHpzc values.

Sample	S_{BET} [a] $m^2\ g^{-1}$	V_t [b] $cm^3\ g^{-1}$	V_{mic} [c] $cm^3\ g^{-1}$	D [d] nm	pHpzc -
NaX	629	0.273	0.219	1.73	9.30
Cu0.01X	467	0.275	0.143	2.35	7.31
Cu0.05X	230	0.155	0.069	2.65	6.27
Cu0.10X	174	0.165	0.025	3.80	5.99
Cu0.15X	149	0.150	0.018	4.05	5.95
Cu0.20X	83	0.090	0.010	4.32	5.94

[a] S_{BET} – specific surface area obtained from N_2 adsorption at 77 K calculated from BET method.
[b] V_t – total pore volume estimated from the volume adsorbed at $p/p_0 \sim 0.98$.
[c] V_{mic} – micropore volume calculated by the *t*-plot method.
[d] D – adsorption average pore diameter 4 V/A from the BET method, pHpzc – pH point of zero charge.

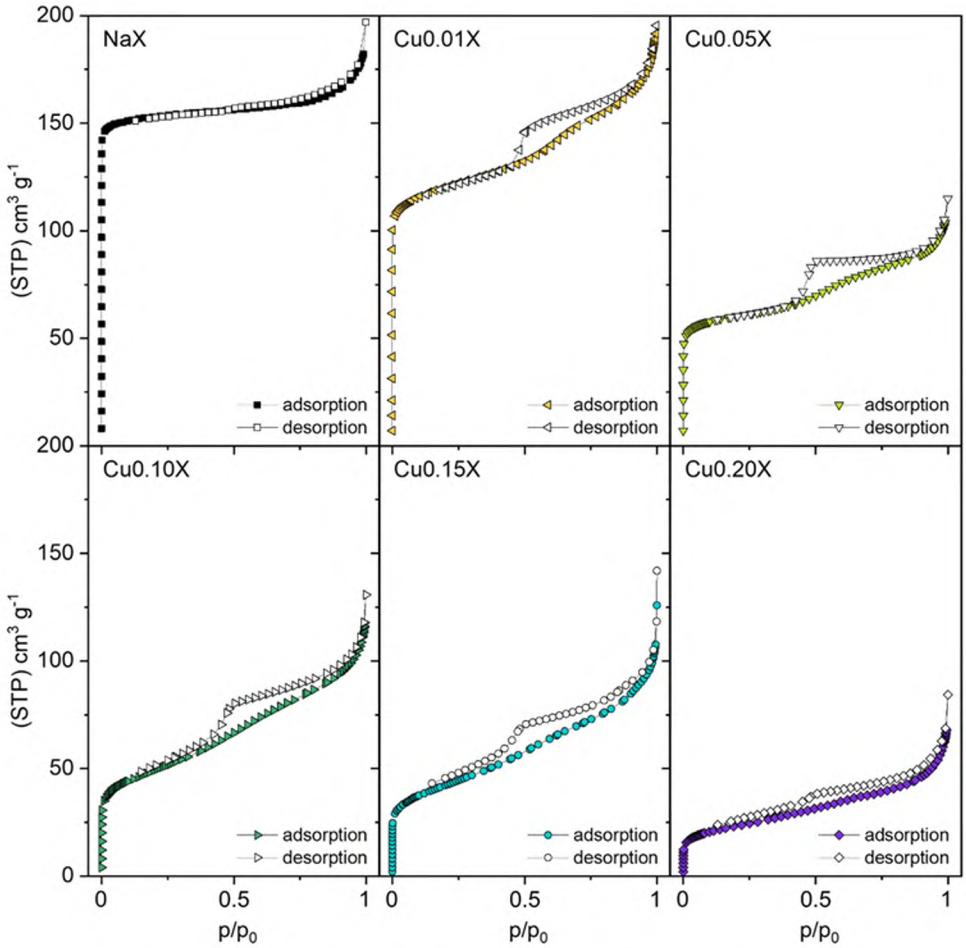

Fig. 2. Low temperature N_2 adsorption-desorption isotherms of the materials at 77 K.

to NaX.

3.1.3. X-ray fluorescence (XRF)

The chemical composition of the materials was obtained from XRF and the results are shown in Table 2. It can be seen that the Si/Al molar ratio remained rather unchanged after modification and ranged from 1.20 to 1.38 compared to the parent NaX (1.31). The increase in Cu $(NO_3)_2$•3 H_2O concentration caused significant changes in the chemical composition of the obtained materials. The Cu content increased as expected with increasing the concentration of $Cu(NO_3)_2$•3 H_2O solution from 4.65% to 20.47% for Cu0.01X and Cu0.20X, respectively. Ion exchange affected the content of Na in the materials, which was completely removed from the zeolite when the concentration of Cu $(NO_3)_2$•3 H_2O was 0.05 M and higher. The high mobility and removal of Na during ion exchange with transition metal cations were also confirmed in other studies [42,53]. The Ca content decreased nearly 3-fold for Cu0.20X when compared to NaX; however, calcium was not removed as efficiently as sodium. The modification had rather insignificant effect on the Fe content, which varied from 0.26% to 0.35%. The K content decreased significantly with increasing concentration of Cu $(NO_3)_2$•3 H_2O solution; however, no significant effect on K removal was observed for concentrations above 0.05 M.

3.1.4. pH point of zero charge (pHpzc)

An important property that also affects the adsorption of anions is the pHpzc of the adsorbents. The pHpzc values of the investigated zeolites are presented in Table 1, and the experimental results are shown in Fig. S1. Anion adsorption is generally favored when the pH of the solution is lower than the pHpzc, as the surface is positively charged. At acidic solution pH (about 3–6), the adsorption mechanism can be complex and is related to both chemical interaction with the adsorbent surface and/or electrostatic attraction [54]. When the pH of the solution is higher than 7, the surface charge becomes more negative. Therefore, electrostatic repulsion decreases the adsorption of phosphate ions. Furthermore, at pH from 7 to about 12, H_2PO_4 ions lose their proton and become divalent ions (HPO_4^{2-}), and at pH of 12 and above, phosphate ions exist as PO_4^{3-}. The combination of those parameters (solution pH, phosphate ions form, and pHpzc of the adsorbent) closely influences and directs the adsorption of phosphate ions. In addition, the DFT studies by Capa-Cobos et al. [55] revealed that hydroxyl groups in the H_2PO_4 ion can interact with hydrogen atoms in FAU zeolite and promote the stability of adsorption complexes.

Two independent analyzes, *i.e.* pHpzc measurements and XRF, revealed a strong positive correlation (R^2 =0.98) between the pHpzc value and the sum of alkali and alkali earth metals (Fig. 3). That correlation confirms that easily exchangeable cations closely influence the pHpzc value of zeolites. During cation exchange, Na was completely removed from the material, while the K and Ca contents were reduced.

3.2. X-ray photoelectron spectroscopy (XPS) for phosphate ions adsorption mechanism studies

The XPS spectra (Fig. 4) were determined for zeolites NaX and

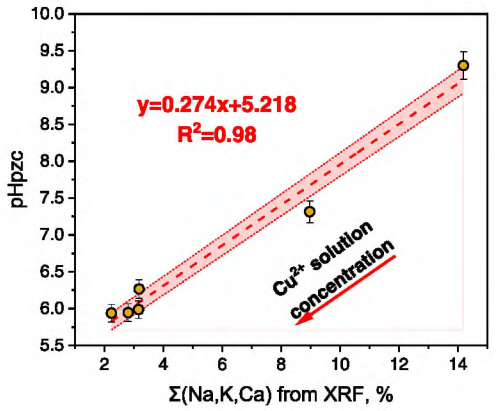

Fig. 3. Correlation of pHpzc of zeolites with sum of alkali and alkali earth metals - Σ(Na,K,Ca) as obtained from XRF (%). The presented data are mean values and standard deviation (<2%) from three replicates of the experiment.

Cu0.05X before and after phosphate ions adsorption to investigate possible adsorption mechanisms. The deconvolution of the O 1 s peak allowed to determine 3 different oxygen species over the zeolite surfaces. The binding energies of 531.3, 532.3, and 533.1 eV were classified as M-O_x lattice silicates, metal-bonded M-OH hydroxyl, and H_2O adsorbed water, respectively [25]. Shifts of the peaks can be clearly observed in the binding energies after adsorption, indicating the occurrence of surface complexation of phosphate species. After adsorption, the peak from M-O_x was 2-fold lower for NaX, while it remained unchanged for Cu0.05X. It also correlated with the Si 2p spectra for NaX, but some significant decrease in the Si 2p peak was also observed for Cu0.05X, implying an additional mechanism of silica coverage over the zeolite surface. Two different types of silica were identified: Si_2O_3 at about 101.9 eV and SiO_2 at 102.5 eV, which was also reported in work by Senthilkumar et al. [56]. On the other hand, the intensity of M-OH was 3-fold higher after adsorption over zeolite NaX and only 1.3-fold lower for Cu0.05X, indicating differences in the electron environment around the surface oxygen atoms [57]. That phenomenon may be related to the higher pHpzc of zeolite NaX (9.30) compared to zeolite Cu0.05X (6.27) [25]. That is caused by the leaching of alkali metals and alkali earth metals into solution during adsorption. For both NaX and Cu0.05X samples, the intensity of the peak at 533.1 eV (H_2O) decreased comparably after adsorption. It can be stated that different adsorption mechanisms occurred for the NaX and Cu0.05X zeolite-solution systems. In the case of zeolite NaX, phosphate ions were adsorbed in the region of silicates, while for zeolite Cu0.05X, other species were involved in adsorption. Hence, one of the possible adsorption mechanisms may be related to the exchange between M-OH and $H_2PO_4^-$ ions [58]. The number of copper species on zeolite Cu0.05X was examined by tracking the Cu 2p region. After adsorption of phosphate ions (Fig. 5b), the intensities of both Cu^0 and Cu^{2+} species increased when compared to sample prior to the adsorption (Fig. 5a), and their peak maxima were detected at 932.8 and 935.0 eV, respectively. Some Cu 3p species were also detected at about 77.5 eV (Fig. 4d_1

Table 2
Bulk (XRF) chemical composition of the investigated zeolites.

Sample	*n*Si/*n*Al	Si	Al	Cu	Ca	Na	K	Fe	Σ (Na, K, Ca)
	–	%	%	%	%	%	%	%	%
NaX	1.31	22.68	16.58	–	6.58	6.93	0.68	0.38	14.19
Cu0.01X	1.28	22.83	17.18	4.65	5.23	3.37	0.37	0.26	8.97
Cu0.05X	1.20	20.65	16.47	15.31	3.05	–	0.13	0.35	3.18
Cu0.10X	1.31	21.18	15.48	16.04	3.04	–	0.12	0.34	3.16
Cu0.15X	1.38	21.16	14.69	17.48	2.73	–	0.08	0.35	2.81
Cu0.20X	1.32	19.93	14.56	20.47	2.16	–	0.08	0.34	2.24

*n*Si/*n*Al – Si/Al molar ratio, Σ(Na, K, Ca) – sum of alkali and alkali earth metals.

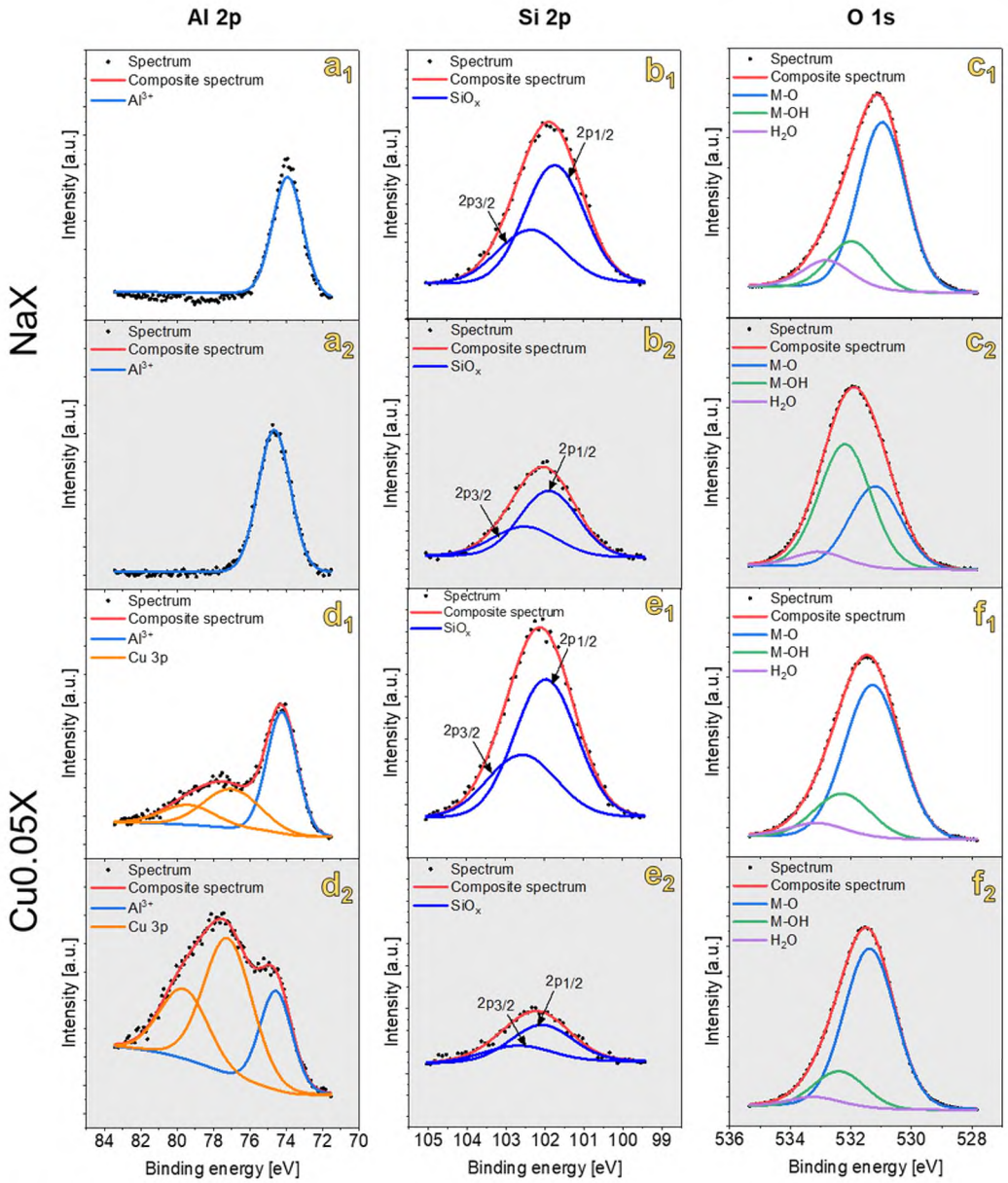

Fig. 4. XPS spectra of Al 2p, Si 2p, and O 1s for zeolites NaX (a-c) and Cu0.05X (d-f), ($_1$) refers to samples before phosphate ion adsorption and ($_2$) to samples after phosphate ions adsorption.

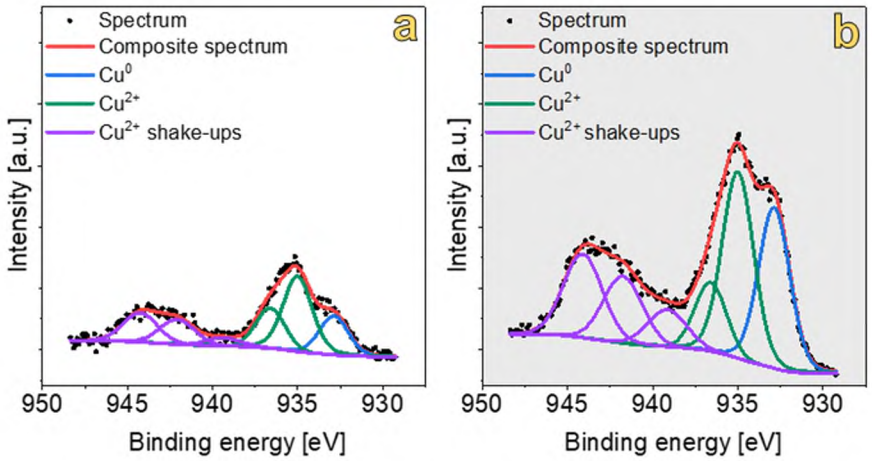

Fig. 5. XPS spectra of Cu 2p for zeolite Cu0.05X before (a) and after (b) phosphate ions adsorption.

and d_2), whose intensities also increased after adsorption. That phenomenon suggests that during adsorption, phosphate ions caused copper extraction from zeolite channels and pores with simultaneous formation of copper phosphate/metaphosphate [59]. Therefore, the decrease in the Si 2p peak for Cu0.05X may be due to the abovementioned copper extraction. A more detailed composition of samples obtained from XPS are shown in Table S3 and he values of peak maxima and their FWHM (full width at half maximum) were compared in Table S4.

After adsorption, a new peak appeared at 132–136 eV for both NaX and Cu0.05X spectra and was assigned as the P 2p region (Fig. 6). The composite spectrum was deconvoluted into 2 peaks: P 2p1/2 and P 2p3/2 were identified. It implies a strong affinity of phosphate ions to zeolite surface [60].

3.3. Adsorption of phosphate ions

3.3.1. Static adsorption of phosphate ions

It was found that ion exchange with Cu^{2+} ions of zeolite NaX had a positive effect on increasing the adsorption capacity of phosphate ions in all zeolite-solution systems (Fig. 7 and Table 3). The experimental data were correlated with Langmuir and Freundlich adsorption isotherm models. The Langmuir model displayed higher correlation with the experimental data (R^2 above 0.98 for most zeolite-solution systems) (Table 3). Therefore, it can be assumed that adsorption occurs over a homogenous surface forming a monolayer of adsorbate (Langmuir isotherm assumption) rather than over a heterogeneous surface forming a multilayer of adsorbate (Freundlich isotherm assumption) [37]. The highest adsorption capacity was observed for Cu0.05X where q_{max} was 87.7 mg (PO_4^{3-}) g^{-1}, as obtained from Langmuir model. Further increase in the concentration of $Cu(NO_3)_2 \bullet 3\ H_2O$ solution used for ion exchange caused a significant decrease in the adsorption capacity. That phenomenon may be the result of some damage to the zeolite structure (Cu0.10, Cu0.15X and Cu0.20X samples) by the formation of $Cu_2(OH)_3NO_3$ species over the zeolite surface (Fig. 1). The performance of the obtained materials indicates that modification of zeolite NaX with Cu^{2+} ions can improve the adsorption properties towards the removal of phosphate ions from aqueous solutions. Some studies address the possible effect of Ca presence in zeolites on the adsorption of phosphate ions. Mitrogiannis et al. [61] treated natural zeolites with $Ca(OH)_2$ and proved that the modification significantly increased the adsorption capacity (from 1.7% to 97.6%). Ca can cause precipitation of phosphate ions into the liquid phase. As shown in XPS analysis (Table S3), Ca was not present in zeolite Cu0.05X after adsorption, and its content was significantly reduced in NaX. Hence, it is possible that some precipitation reactions also take place. What more, the pH of the solution after adsorption was higher for the NaX zeolite-solution system (7.78) compared to the Cu0.05X zeolite-solution system (6.65), despite adjusting the pH value

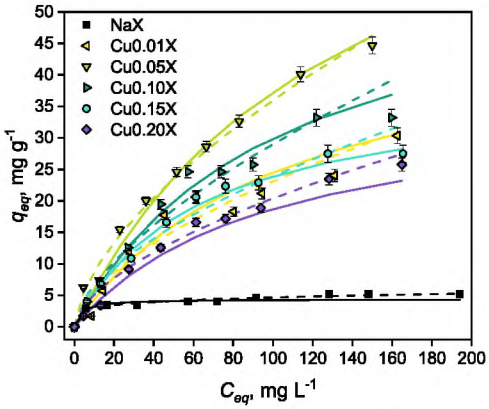

Fig. 7. Adsorption isotherms of the investigated materials – the solid line refers to the correlation with the Langmuir model and the dashed line refers to the correlation with the Freundlich model. The presented data (points) are mean values and standard deviation (<5%) from three replicates of the experiment. T = 25 °C; t = 24 h; zeolite/solution ratio= 1 g L^{-1}; initial pH= 5.00.

Table 3
The isothermal adsorption fitting parameters of Freundlich and Langmuir models.

Sample	Adsorption model						
	Langmuir				Freundlich		
	q_{max}	K_L	R^2	R_L	K_F	$1/n$	R^2
NaX	4.38	0.327	0.921	0.015	2.04	0.180	0.934
Cu0.01X	50.76	0.009	0.966	0.357	1.44	0.602	0.907
Cu0.05X	87.72	0.007	0.998	0.417	2.13	0.614	0.969
Cu0.10X	60.24	0.010	0.994	0.333	1.54	0.638	0.948
Cu0.15X	39.06	0.016	0.987	0.238	1.66	0.580	0.961
Cu0.20X	36.77	0.010	0.981	0.333	1.33	0.593	0.981

R_L parameter was calculated for C_0= 200 mg (PO_4^{3-}) g^{-1}, R^2 – coefficient value, q_{max} – maximum adsorption capacity (mg g^{-1}), $1/n$ – heterogeneity factor, K_L – Langmuir model constant (L mg^{-1}), K_F – Freundlich model constant ($mg^{1-1/n}\ L^{1/n}\ g^{-1}$), Equation – linear form of the Langmuir and Freundlich models.

to 5.00. Precipitation as calcium phosphate is one of the possible mechanisms during the removal of phosphate ions [58]. The R_L parameter calculated for all adsorption systems allowed to conclude that adsorption was favorable in all cases. The R_L value was 0.015 for NaX, while it varied from 0.238 to 0.417 for modified zeolites. The low value of that parameter for zeolite NaX suggests that adsorption was much less favorable than for Cu ion-exchanged zeolites.

The adsorption capacities of the modified zeolites given in this study

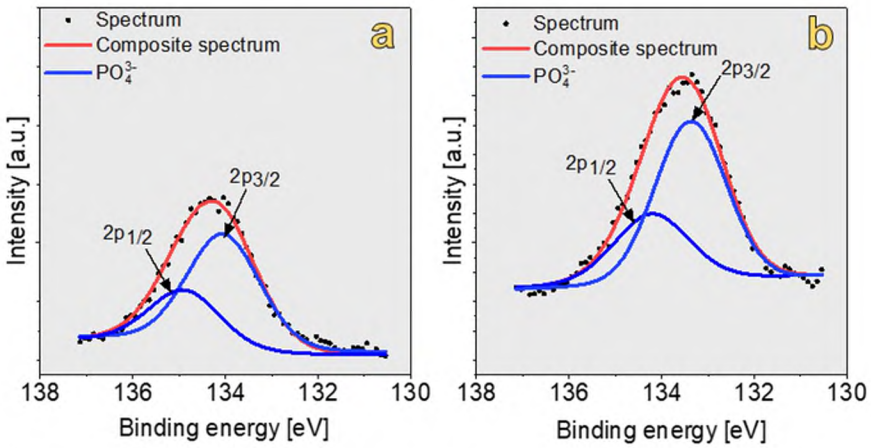

Fig. 6. XPS spectra of P 2p after adsorption of phosphate ions over zeolites NaX (a) and Cu0.05X (b).

were compared with literature data and are presented in Table 4.

As the adsorption was conducted at pH of 5.00 and after the adsorption of phosphate ions the solution pH increased much below the pHpzc values of the materials (see Table 1), the zeolites should maintain positive protonated surface. Hence, the mechanism of adsorption can be ligand exchange or electrostatic attraction as shown in Eqs. (1)–(3) [25]:

$$\text{Zeolite-Cu-OH} + H^+ = \text{Zeolite-Cu-OH}_2^+ \quad (1)$$

$$\text{Zeolite-Cu-OH}_2^+ + H_2PO_4^- = (\text{Zeolite-Cu-OH}_2)^+(H_2PO_4)^- \quad (2)$$

$$\text{Zeolite-Cu-OH} + H_2PO_4^- = \text{Zeolite-Cu-}H_2PO_4 + OH^- \quad (3)$$

3.3.2. Kinetic adsorption of phosphate ions

The results of kinetic adsorption studies were correlated with the kinetic models and are shown in Fig. 8a and b, and the kinetic model parameters are compared in Table 5. Kinetic adsorption studies allow to determine the adsorption rate, the time needed to reach the equilibrium, and to investigate possible adsorption mechanisms. However, the obtained results should be interpreted with caution [66,67]. It can be noted that for both NaX and Cu0.05X zeolite-solution systems, the pseudo second order mechanism displayed the highest correlation (R^2 =1.00). It is often assumed that the correlation of the data with the pseudo second order model suggests chemisorption between the adsorbate and the adsorbent active sites, involving valence forces and/or electron exchange. The equilibrium values obtained from the pseudo second order model were 28.82 and 5.91 mg (PO_4^{3-}) g^{-1} for Cu0.05X and NaX, respectively. Hence, after ion exchange, a significant increase in the adsorption capacity was obtained compared to the parent zeolite NaX (about 4.9-fold). The phosphate ions removal efficiency increased from 5.4% for zeolite NaX to 32.3% for zeolite Cu0.05X (t = 24 h, T = 25 °C, C_0 =80 mg (PO_4^{3-}) L^{-1}). The pseudo first order model had rather weak correlation with the experimental data, probably due to the rapid initial adsorption followed by a long time to achieve equilibrium caused by occupancy of adsorption sites. It can be seen that the equilibrium values obtained from the Lagergren model differ from those obtained from the pseudo second order model. A near equilibrium value was established in about 12 h. To better understand the adsorption kinetics, other models were also employed. The correlation of the Bangham model allowed to conclude that adsorption in pores was not the limiting step (R^2 below 0.99). Also, the S_{BET} of zeolite NaX was significantly higher (629 m^2 g^{-1}) when compared to zeolite Cu0.05X (230 m^2 g^{-1}). That implies that other mechanisms are involved in adsorption, which was also confirmed by XPS measurements. Furthermore, 2 linearity steps of adsorption were found from the Weber-Morris model (Fig. 8b). The first linearity step for both NaX and Cu0.05X adsorption systems exhibited a negative C_i intercept value. Such a phenomenon is explained by the lack of boundary layer limitations, hence phosphate ions are easily accessible to adsorption sites over the adsorbent surface [68]. Phosphate ions are rapidly transferred into the porous material, and the second linearity step represents slow penetration into the pores inside the material where adsorption occurs [69]. From the Elovich model it can be concluded that adsorption over Cu0.05X zeolite may be related to chemisorption, since the correlation value (R^2) was 0.96. The occurrence of electrostatic attraction of phosphate ions to the surface active sites and/or the formation of copper phosphate/metaphosphate were the guiding mechanism of adsorption. Some studies also assumed heterogeneous adsorption as the Elovich model coefficient increases [70]. In the Elovich model, the constant a reflects the initial adsorption rate [71]. The greater value of the constant a from the Elovich equation obtained for NaX (3.335 mg g^{-1} min^{-1}) compared to Cu0.05X (2.458 mg g^{-1} min^{-1}) may be related to the rather rapid initial adsorption of phosphate ions over the NaX zeolite. After the rapid initial adsorption, the active sites of zeolite NaX were no longer able to adsorb greater amounts of phosphate ions and reach the equilibrium value. The value of the constant b is

Table 4
Comparison of the adsorption capacities of various zeolites toward phosphate ions removal and adsorption parameters.

Zeolite	Modification	Adsorption capacity (Langmuir), mg g^{-1}	Adsorption parameters	Ref.
Na-A La-A Na-P1 La-P1	Fly-ash-derived zeolites Na-A and Na-P1 modified by ion exchange with La^{3+}	25.55 48.95 14.37 61.12	Solution concentrations: 12.5–200 mg (PO_4^{3-}) L^{-1}; Zeolite/solution ratio: 1 g L^{-1}; Contact time: 24 h; Initial solution pH: 5.00; Temperature: 25 °C;	[21]
HUD Al-HUD	Commercial HUD zeolite and HUD zeolite modified by ion exchange with Al^{3+}	79.4 75.8	Solution concentrations: 50–300 mg (PO_4^{3-}) L^{-1}; Zeolite/solution ratio: 1 g L^{-1}; Contact time: 168 h; Initial solution pH: 5.70; Temperature: 25 °C;	[62]
Zeolite-A Fe-zeolite-A	Iron introduced into zeolite A during synthesis followed by calcination of the material	- 18.15	Solution concentrations: 2–20 mg (PO_4^{3-}) L^{-1}; Zeolite/solution ratio: 4 g L^{-1}; Contact time: 10 min; Initial solution pH: 5.00; Temperature: -;	[26]
ZSM-5 La-ZSM-5	Commercial zeolite ZSM-5 ion-exchanged with La^{3+} followed by calcination of the material	59.8 106.2	Solution concentrations: 10–700 mg (PO_4^{3-}) L^{-1}; Zeolite/solution ratio: 5 g L^{-1}; Contact time: 3 h; Initial solution pH: 6.00; Temperature: 22 °C;	[63]
Zeolite-A	Zeolite-A synthesized from clay by alkaline fusion and crystallized at 70 °C	52.9	Solution concentrations: 50–1000 mg (P) L^{-1}; Zeolite/solution ratio: 6.7 g L^{-1}; Contact time: 4 h; Initial solution pH: 5.00; Temperature: 25 °C;	[64]
Zeolite+MAL	Zeolite loaded with Mg-Al-La ternary hydroxides (12.5 wt% loading of La)	80.8	Solution concentrations: 10–100 mg (P) L^{-1}; Zeolite/solution ratio: 0.2 g L^{-1}; Contact time: 6 h; Initial solution pH: 6.60; Temperature: 25 °C;	[65]
Na-X Cu0.05X	Fly-ash-derived zeolite NaX	4.38 87.72	Solution concentrations:	This study

(continued on next page)

Table 4 (*continued*)

Zeolite	Modification	Adsorption capacity (Langmuir), mg g^{-1}	Adsorption parameters	Ref.
	modified by ion exchange with Cu^{2+} ions		10–200 mg (PO_4^{3-}) L^{-1}; Zeolite/solution ratio: 1 g L^{-1}; Contact time: 24 h; Initial solution pH: 5.00; Temperature: 25 °C;	

related to the extent of surface coverage and the activation energy and/or desorption rate [72]. That value was much lower for the Cu0.05X zeolite-solution system. Hence, the connection of phosphate ions onto zeolite Cu0.05X seems to be more favored than for zeolite NaX.

3.3.3. *The effect of adsorbent dose and adsorption temperature*

To get more information about the effect of operating conditions on phosphate ions absorption in the investigated systems, additional single-point adsorption experiments were carried out. Table 6 compares the effect of adsorbent dose on phosphate ions adsorption. The graphical presentation of the results is given in Fig. S2. As can be seen, the adsorption capacity decreased for both zeolites NaX and Cu0.05X with the increased absorbent dose, *i.e.* from 1 to 3 g L^{-1}. For zeolite NaX, the adsorption capacity decreased in the order of 4.4, 3.2, and 2.5 mg (PO_4^{3-}) g^{-1} for adsorbent dose 1, 2, and 3, respectively. Similarly, for zeolite Cu0.05X, the adsorption capacity of the material decreased in the same order: 24.6, 22.9, and 17.2 mg (PO_4^{3-}) g^{-1}, respectively. The increased zeolite dose improved the availability of surface adsorption sites and more phosphate ions were transferred into the zeolite matrix, making the percentage removal higher. That phenomenon was also reported in the literature [73]. A significant effect of zeolite NaX ion exchange with copper nitrate on the increase in phosphate ions removal can be observed. For the parent zeolite NaX, the increased dose had a weak effect on phosphate ions removal, which was 5.4%, 8.1%, and 9.6% for doses 1, 2, and 3 g L^{-1}, respectively. In contrast, for zeolite Cu0.05X, the dose increased from 1 to 2 g L^{-1} significantly enhanced the removal of phosphate ions from 32.3% to 58.1%. Increasing the zeolite dose to 3 g L^{-1} promoted further increase in the percentage removal of phosphate ions to 65.4%, but the rate was much lower than for the zeolite dose increased from 1 to 2 g L^{-1}.

As can be found in the literature, the temperature is one of the key factors of adsorption process, that can affect the performance of the adsorbent [21,74,75]. Single-point adsorption experiment was employed to investigate the effect of adsorption temperature on the removal of phosphate ions. Table 6. shows that the temperature increase from 25 °C to 40 °C had almost no effect on the adsorption of phosphate ions from the solution for both zeolites NaX and Cu0.05X. After heating to 40 °C, the removal of phosphate ions decreased slightly from 5.4% to 5.2% and from 32.3% to 30.9% for zeolites NaX and Cu0.05X, respectively. When the adsorption was performed at 18 °C, the removal of phosphate ions was decreased (3.0% and 26.5% for zeolite NaX and Cu0.05X, respectively). A similar observation was also presented by Xu et al. [76]. On the other hand, Goscianska et al. [21] reported that the

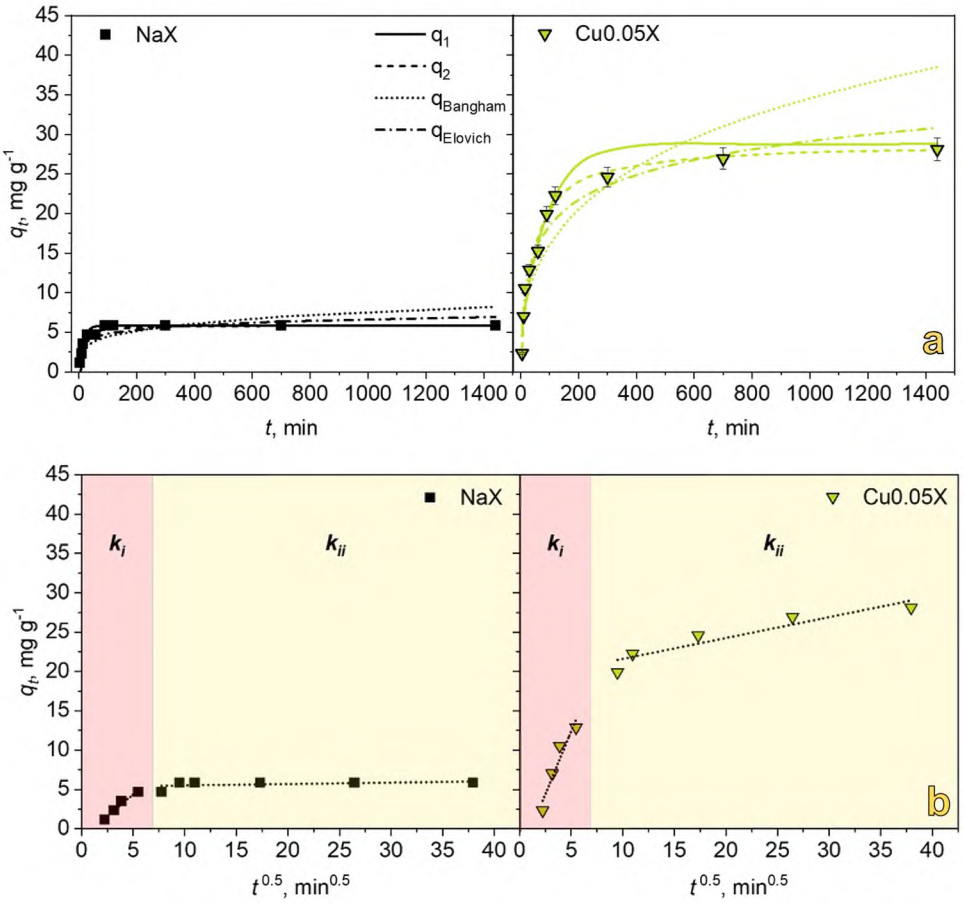

Fig. 8. Correlation of adsorption kinetic models (q_1 – pseudo first order, q_2 – pseudo second order, $q_{Bangham}$ – Bangham model, $q_{Elovich}$ – Elovich model) (a), and Weber-Morris model (b) with experimental data of phosphate ion adsorption over zeolites NaX and Cu0.05X. The presented data (points) are mean values and standard deviation (<5%) from three replicates of the experiment. C_0 = 80 mg(PO_4^{3-}) L^{-1}; T = 25 °C; zeolite/solution ratio= 1 g L^{-1}; initial pH= 5.00.

Table 5
Adsorption kinetic parameters.

Model	Kinetic parameters	Sample	
		NaX	Cu0.05X
Pseudo first order	q_{exp}, mg g^{-1}	5.91	28.82
	q_{eq}, mg g^{-1}	9.47	24.25
	k_1, min^{-1}	0.074	0.011
	R^2	0.87	0.97
Pseudo second order	q_{eq}, mg g^{-1}	5.91	28.82
	k_2, g mg^{-1} min^{-1}	$181.6 \bullet 10^{-4}$	$8.3 \bullet 10^{-4}$
	R^2	1.00	1.00
Bangham	α	0.239	0.403
	k_0, L^2 g^{-1}	$1.89 \bullet 10^{-3}$	$3.40 \bullet 10^{-3}$
	R^2	0.66	0.80
Elovich	a, mg g^{-1} min^{-1}	3.335	2.458
	b, g mg^{-1}	1.252	0.215
	R^2	0.76	0.96
Weber-Morris	k_i, mg g^{-1} $min^{-0.5}$	1.088	3.192
	C_i, mg g^{-1}	-1.081	-3.569
	R^2	0.97	0.91
	k_{ii}, mg g^{-1} $min^{-0.5}$	0.018	0.265
	C_{ii}, mg g^{-1}	5.337	18.950
	R^2	0.19	0.88

Table 6
Effects of adsorbent dose and adsorption temperature on adsorption capacity and percentage removal of phosphate ions.

Operating conditions	Sample	
	NaX	Cu0.05X
	Adsorption capacity, mg (PO_4^{3-}) g^{-1} / Removal of PO_4^{3-}, %	
Adsorbent dose, g L^{-1}		
1	4.1 ± 0.1 / 5.4	24.6 ± 0.5 / 32.3
2	3.2 ± 0.1 / 8.1	22.9 ± 0.5 / 58.1
3	2.5 ± 0.1 / 9.6	17.2 ± 0.4 / 65.4
Adsorption temperature, °C		
18	3.0 ± 0.1 / 4.0	21.0 ± 0.4 / 26.5
25	4.1 ± 0.1 / 5.4	24.6 ± 0.5 / 32.3
40	4.1 ± 0.1 / 5.1	24.3 ± 0.5 / 30.9

Adsorbent dose: T = 25 °C, t = 24 h, C_0= 80 mg (PO_4^{3-}) L^{-1}, initial pH= 5.00; Adsorption temperature: adsorbent dose= 1 g L^{-1}; t = 24 h, C_0= 80 mg (PO_4^{3-}) L^{-1}, initial pH= 5.00.

adsorption temperature increase from 25 to 60 °C slightly increased the adsorption capacity (by 11%) of the investigated lanthanum-modified zeolites. That behavior was explained by the improved mobility of phosphate ions in the solution and easier access to zeolites active sites. Wan et al. [74] observed that with an increase in temperature, cation exchange process can be favored, resulting in higher Ca^{2+} ions concentration in the solution, which can be also involved in the adsorption *via* precipitation as calcium phosphates. In the case of zeolites NaX and Cu0.05X, the amount of Ca was lower after adsorption (Table S3). Increase in phosphate ions removal was observed when the temperature was increased from 18 to 25 °C. Lower amount of calcium in the samples after adsorption (at 25 °C – see Table S3) suggests, that precipitation can be involved in adsorption as shown in Eq. (4):

$$Ca^{2+} + 2H_2PO_4^- = Ca(H_2PO_4)_2\downarrow \quad (4)$$

However, further increase in adsorption temperature from 25 to 40 °C had rather negligible effect on the phosphate ions removal probably due to rather its low amount in the samples. Drop in adsorption capacity for samples incubated at 18 °C was probably due to the lower mass transfer and/or inhibited release of Ca^{2+} ions. Hence, the optimal temperature for adsorption of phosphate ions was found to be 25 °C.

3.4. Leaching test

Leaching tests were performed using zeolites NaX and Cu0.05X to identify the fraction transferred into the aqueous solution. In order to determine the potential application of the adsorbent, it is important to know the migration characteristics of substances added to the aqueous environment. The results obtained were compared with distilled water (H_2O) used for the leaching test and are presented in Table S5. It was found that the chemical composition of water was free from common contaminants, whose levels were below detection limits. Also, the chemical composition of water leachate after the leaching test for zeolites NaX and Cu0.05X showed trace levels of almost all components. In the zeolite NaX leachate, small amounts of Al (5.99 mg L^{-1}), Fe (0.028 mg L^{-1}), Na (11.19 mg L^{-1}), and Si (7.65 mg L^{-1}) were detected. In contrast, for zeolite Cu.0.05X, the composition of leachate was much less diversified. Significantly lower amounts of all components imply greater stability of the material. Copper was present in the leachate of zeolite Cu0.05X, but its content was very low (121 ppb). Thus, it proves that copper is rather well-bonded with the zeolite structure. Some leaching of alumina and silica occurred for both zeolites NaX and Cu0.05X, but their low values indicate that the zeolite matrix was stable [77]. Furthermore, the matrix of zeolite Cu0.05X appeared to be even more stable than that of NaX because the leachate composition (Al and Si) was much less diversified. Small amounts of sodium were identified in the leachate of Cu0.05X, whose presence was not confirmed in XRF analysis (Table 2), probably due to detection limits. In the case of the zeolite NaX leachate, the presence of sodium may be due to post-synthesis residuals.

3.5. Implication of practical application

Summarizing the present study, we would like to highlight some important findings. The results of phosphates ion adsorption using fly-ash-derived zeolite X showed that the introduction of copper by ion exchange caused: (*i*) the removal of alkali and alkali earth metals from the zeolite matrix, which led to decrease in the pHpzc of the materials; (*ii*) changes in the textural properties of zeolites – wider pores and S_{BET} decrease; (*iii*) the increase in the adsorption capacity towards the removal of phosphate ions from aqueous solutions. It should be noted that all modified zeolites had better adsorption capacities than the parent zeolite NaX. The application of zeolite Cu0.05X in adsorption ensured the highest efficiency in removing phosphate ions.

It appears that the production of zeolites from fly ashes and their modification with copper by ion exchange can be an efficient method to utilize wastes as raw materials in the preparation of value-added products. Adsorption of phosphate ions onto zeolites can also be further investigated in terms of fertilizer production [78,79]. The use of fertilizers with the addition of functionalized materials, such as zeolites enriched with phosphate ions, is a fully innovative method of rational management of soil resources. Also, the application of synthetic zeolites from fly ash to the soil can negatively affect plant growth and yield as a result of a higher sodium content after alkaline hydrothermal synthesis [80]. Ion exchange with Cu^{2+} ions, even at low concentrations, can remove Na from the zeolite material. However application of materials containing Cu should be made with cautions. The permissible levels of Cu in soil should not exceed 100 mg kg^{-1} to allow healthy plant growth and avoid contamination of environment [81].

Another important possibility of using phosphorus-enriched zeolites is their application for the regeneration of spent catalysts [59]. Much attention has been given to improving the stability and chemical resistance of catalysts used for selective catalytic reduction (SCR) of NO_x. The presence of phosphorus has been found to be an efficient strategy to protect active sites from, *inter alia*, poisoning with SO_2 [82]. Low phosphorus concentrations used for catalyst regeneration reduce the content of CuO species and inhibit the problem of side reactions (NH_3 oxidation) [59]. On the other hand, Chen et al. [83] proved that the resistance of Cu-SSZ-13 catalyst to sulfur poisoning was reduced with the increased phosphorus load. Furthermore, the NO conversion also decreased drastically. Therefore, it is important to investigate the effect

of the physicochemical and structural properties of the catalysts, the methods of phosphorus incorporation, as well as phosphorus concentration on the catalytic activity.

4. Conclusions

This study showed that Cu ion-exchanged zeolites X derived from fly ash were efficient adsorbents of phosphate ions from aqueous solutions. The possible adsorption mechanism was estimated through the formation of copper phosphate based on XPS analysis. The optimization of zeolite X modification concentrated on the influence of the initial copper nitrate solution concentration. The increased concentration of Cu $(NO_3)_2 \bullet 3\ H_2O$ solution applied for ion exchange noticeably affected both the textural and morphological properties of obtained zeolites. As a result, the optimal concentration for the modification of zeolite X towards phosphate ions adsorption was 0.05 M of $Cu(NO_3)_2 \bullet 3\ H_2O$ solution. Further increase in the concentration of copper nitrate solution above 0.10 M decreased the adsorption capacity due to partial pore blockage. After ion exchange with copper nitrate, zeolites exhibited lower pHpzc due to removal of alkali and alkali earth metals. A strong positive correlation was also found between pHpzc and the content of alkali and alkali earth metals in the materials.

The maximum adsorption capacity of 87.7 mg $(PO_4^{3-})\ g^{-1}$ was obtained for zeolite Cu0.05X. Additionally, the adsorption capacity determined for that zeolite was about 20 times higher as compared to that of the parent zeolite NaX. Accordingly, the adsorption properties of Cu ion-exchanged zeolites can be improved. Single-point adsorption experiments were conducted to investigate the effects of adsorbent dose and adsorption temperature. As the adsorbent dose increased, the percentage removal of phosphate ions also increased, but this change was more noticeable for Cu0.05X than for the parent zeolite NaX. As the adsorption temperature increased from 18 to 25 °C the adsorption capacity slightly increased, however further increase in the temperature to 40 °C had almost no effect on phosphate ions removal. The leaching test was performed to identify the potential risk of applying adsorbents. Despite trace presence of alumina, silica, and sodium, zeolites remained stable in the aqueous environment. Our study demonstrates a novel, environmentally friendly, and also highly efficient adsorbents for removal of phosphate ions from aqueous solutions, which can potentially prevent emergence of eutrophication or be further applied for production of fertilizers.

CRediT authorship contribution statement

Jakub Mokrzycki: Conceptualization, Methodology, Software, Validation, Formal analysis, Investigation, Data curation, Writing – original draft, Writing – review & editing, Visualization. **Monika Fedyna:** Methodology, Software, Validation, Formal analysis, Investigation, Data curation, Writing – original draft, Writing – review & editing, Visualization. **Mateusz Marzec:** Methodology, Software, Validation, Formal analysis, Investigation, Data curation, Writing – original draft, Writing – review & editing, Visualization. **Justyna Szerement:** Methodology, Formal analysis, Investigation, Data curation, Writing – original draft, Writing – review & editing. **Rafał Panek:** Methodology, Software, Validation, Formal analysis, Investigation, Data curation, Writing – original draft, Writing – review & editing. **Agnieszka Klimek:** Writing – original draft, Writing – review & editing. **Tomasz Bajda:** Methodology, Investigation, Resources, Writing – review & editing, Supervision, Project administration, Funding acquisition. **Monika Mierzwa-Hersztek:** Methodology, Resources, Writing – review & editing, Supervision, Project administration, Funding acquisition.

Declaration of Competing Interest

The authors declare that they have no known competing financial interests or personal relationships that could have appeared to influence the work reported in this paper.

Data availability

Data will be made available on request.

Acknowledgments

The study was conducted under the project "Fly ashes as the precursors of functionalized materials for applications in environmental engineering, civil engineering and agriculture"—the project is carried out within the TEAM-NET programme of the Foundation for Polish Science POIR.04.04.00-00-14E6/18-00.

Appendix A. Supplementary material

Supplementary data associated with this article can be found in the online version at doi:10.1016/j.jece.2022.108567.

References

[1] P.J.A. Withers, C. Neal, H.P. Jarvie, D.G. Doody, Agriculture and eutrophication: where do we go from here? Sustainability Vol. 6 (2014) 5853–5875, https://doi.org/10.3390/SU6095853.
[2] Y. Yang, H. Zhu, X. Xu, L. Bao, Y. Wang, H. Lin, C. Zheng, Construction of a novel lanthanum carbonate-grafted ZSM-5 zeolite for effective highly selective phosphate removal from wastewater, Microporous Mesoporous Mater. 324 (2021), 111289, https://doi.org/10.1016/J.MICROMESO.2021.111289.
[3] S. Salehi, M. Hosseinifard, Highly efficient removal of phosphate by lanthanum modified nanochitosan-hierarchical ZSM-5 zeolite nanocomposite: characteristics and mechanism, Cellulose 27 (2020) 4637–4664, https://doi.org/10.1007/S10570-020-03094-W/FIGURES/9.
[4] W. Shi, Y. Fu, W. Jiang, Y. Ye, J. Kang, D. Liu, Y. Ren, D. Li, C. Luo, Z. Xu, Enhanced phosphate removal by zeolite loaded with Mg–Al–La ternary (hydr)oxides from aqueous solutions: performance and mechanism, Chem. Eng. J. 357 (2019) 33–44, https://doi.org/10.1016/J.CEJ.2018.08.003.
[5] M. Zamparas, A. Gianni, P. Stathi, Y. Deligiannakis, I. Zacharias, Removal of phosphate from natural waters using innovative modified bentonites, Appl. Clay Sci. 62–63 (2012) 101–106, https://doi.org/10.1016/J.CLAY.2012.04.020.
[6] E. Rosales, G. del Olmo, C. Calero Preciado, I. Douterelo, Phosphate dosing in drinking water distribution systems promotes changes in biofilm structure and functional genetic diversity, Front. Microbiol. 11 (2020), https://doi.org/10.3389/FMICB.2020.599091/FULL.
[7] M.R. Awual, Efficient phosphate removal from water for controlling eutrophication using novel composite adsorbent, J. Clean. Prod. 228 (2019) 1311–1319, https://doi.org/10.1016/J.JCLEPRO.2019.04.325.
[8] M. Molinos-Senante, F. Hernández-Sancho, R. Sala-Garrido, M. Garrido-Baserba, Economic feasibility study for phosphorus recovery processes, Ambio 40 (2011) 408–416, https://doi.org/10.1007/S13280-010-0101-9/TABLES/4.
[9] M.N. Quang, T. Rogers, J. Hofman, A.B. Lanham, New framework for automated article selection applied to a literature review of enhanced biological phosphorus removal, PLOS ONE 14 (2019), e0216126, https://doi.org/10.1371/JOURNAL.PONE.0216126.
[10] L.E. De-Bashan, Y. Bashan, Recent advances in removing phosphorus from wastewater and its future use as fertilizer (1997–2003), Water Res. 38 (2004) 4222–4246, https://doi.org/10.1016/J.WATRES.2004.07.014.
[11] P. Loganathan, S. Vigneswaran, J. Kandasamy, N.S. Bolan, Removal and recovery of phosphate from water using sorption, Crit. Rev. Environ. Sci. Technol. 44 (2014) 847–907, https://doi.org/10.1080/10643389.2012.741311.
[12] M. Wiśniewska, T. Urban, S. Chibowski, G. Fijałkowska, M. Medykowska, A. Nosal-Wiercińska, W. Franus, R. Panek, K. Szewczuk-Karpisz, Investigation of adsorption mechanism of phosphate(V) ions on the nanostructured Na-A zeolite surface modified with ionic polyacrylamide with regard to their removal from aqueous solution, Appl. Nanosci. 10 (2020) 4475–4485, https://doi.org/10.1007/S13204-020-01397-9/TABLES/2.
[13] M. Saifuddin, J. Bae, K.S. Kim, Role of Fe, Na and Al in Fe-Zeolite-A for adsorption and desorption of phosphate from aqueous solution, Water Res. 158 (2019) 246–256, https://doi.org/10.1016/J.WATRES.2019.03.045.
[14] S. Salehi, M. Hosseinifard, Highly efficient removal of phosphate by lanthanum modified nanochitosan-hierarchical ZSM-5 zeolite nanocomposite: characteristics and mechanism, Cellulose 27 (2020) 4637–4664, https://doi.org/10.1007/S10570-020-03094-W/FIGURES/9.
[15] K. Zhang, L. van Dyk, D. He, J. Deng, S. Liu, H. Zhao, Synthesis of zeolite from fly ash and its adsorption of phosphorus in wastewater, Green Process. Synth. 10 (2021) 349–360, https://doi.org/10.1515/GPS-2021-0032/ASSET/GRAPHIC/J_GPS-2021-0032_FIG_008.JPG.
[16] L.F. Capa-Cobos, X. Jaramillo-Fierro, S. González, Computational study of the adsorption of phosphates as wastewater pollutant molecules on faujasites, Processes Vol. 9 (2021) 1821, https://doi.org/10.3390/PR9101821.

[17] J. He, Y. Xu, W. Wang, B. Hu, Z. Wang, X. Yang, Y. Wang, L. Yang, Ce(III) nanocomposites by partial thermal decomposition of Ce-MOF for effective phosphate adsorption in a wide pH range, Chem. Eng. J. 379 (2020), 122431, https://doi.org/10.1016/J.CEJ.2019.122431.
[18] M. Fathy, M.A. Zayed, A.M.G. Mohamed, Phosphate adsorption from aqueous solutions using novel Zn Fe/Si MCM-41 magnetic nanocomposite: characterization and adsorption studies, Nanotechnol. Environ. Eng. 4 (2019) 1–12, https://doi.org/10.1007/S41204-019-0061-7/FIGURES/14.
[19] J.Y. Kim, M.S. Balathanigaimani, H. Moon, Adsorptive removal of nitrate and phosphate using MCM-48, SBA-15, chitosan, and volcanic pumice, Water Air Soil Pollut. 226 (2015) 1–11, https://doi.org/10.1007/S11270-015-2692-Z/TABLES/5.
[20] W. Huang, D. Li, Y. Zhu, K. Xu, J. Li, B. Han, Y. Zhang, Fabrication of Fe-coordinated diamino-functionalized SBA-15 with hierarchical porosity for phosphate removal, Mater. Lett. 99 (2013) 154–157, https://doi.org/10.1016/J.MATLET.2013.03.017.
[21] J. Goscianska, M. Ptaszkowska-Koniarz, M. Frankowski, M. Franus, R. Panek, W. Franus, Removal of phosphate from water by lanthanum-modified zeolites obtained from fly ash, J. Colloid Interface Sci. 513 (2018) 72–81, https://doi.org/10.1016/j.jcis.2017.11.003.
[22] J. Cieśla, W. Franus, M. Franus, K. Kedziora, J. Gluszczyk, J. Szerement, G. Jozefaciuk, Environmental-friendly modifications of zeolite to increase its sorption and anion exchange properties, physicochemical studies of the modified materials, Materials Vol. 12 (2019) 3213, https://doi.org/10.3390/MA12193213.
[23] W. Zou, X. Feng, W. Wei, Y. Zhou, R. Wang, R. Zheng, J. Li, S. Luo, H. Mi, H. Chen, Converting spent LiFePO4 battery into zeolitic phosphate for highly efficient heavy metal adsorption, Inorg. Chem. 60 (2021) 9496–9503, https://doi.org/10.1021/ACS.INORGCHEM.1C00614/ASSET/IMAGES/LARGE/IC1C00614_0005.JPEG.
[24] C. Wang, J. Li, X. Sun, L. Wang, X. Sun, Evaluation of zeolites synthesized from fly ash as potential adsorbents for wastewater containing heavy metals, J. Environ. Sci. 21 (2009) 127–136, https://doi.org/10.1016/S1001-0742(09)60022-X.
[25] Y. He, H. Lin, Y. Dong, L. Wang, Preferable adsorption of phosphate using lanthanum-incorporated porous zeolite: characteristics and mechanism, Appl. Surf. Sci. 426 (2017) 995–1004, https://doi.org/10.1016/J.APSUSC.2017.07.272.
[26] M. Saifuddin, J. Bae, K.S. Kim, Role of Fe, Na and Al in Fe-Zeolite-A for adsorption and desorption of phosphate from aqueous solution, Water Res. 158 (2019) 246–256, https://doi.org/10.1016/J.WATRES.2019.03.045.
[27] D. Guaya, C. Valderrama, A. Farran, C. Armijos, J.L. Cortina, Simultaneous phosphate and ammonium removal from aqueous solution by a hydrated aluminum oxide modified natural zeolite, Chem. Eng. J. 271 (2015) 204–213, https://doi.org/10.1016/J.CEJ.2015.03.003.
[28] G. Italiya, M.H. Ahmed, S. Subramanian, Titanium oxide bonded zeolite and bentonite composites for adsorptive removal of phosphate, Environ. Nanotechnol. Monit. Manag. 17 (2022), 100649, https://doi.org/10.1016/J.ENMM.2022.100649.
[29] M.A. Salam, M. Mokhtar, S.M. Albukhari, D.F. Baamer, L. Palmisano, A. A. AlHammadi, M.R. Abukhadra, Synthesis of zeolite/geopolymer composite for enhanced sequestration of phosphate (PO43−) and ammonium (NH4+) ions; equilibrium properties and realistic study, J. Environ. Manag. 300 (2021), 113723, https://doi.org/10.1016/J.JENVMAN.2021.113723.
[30] Y. Abdellaoui, H. Abou Oualid, A. Hsini, B. el Ibrahimi, M. Laabd, M. el Ouardi, G. Giácoman-Vallejos, P. Gamero-Melo, Synthesis of zirconium-modified Merlinoite from fly ash for enhanced removal of phosphate in aqueous medium: experimental studies supported by Monte Carlo/SA simulations, Chem. Eng. J. 404 (2021), 126600, https://doi.org/10.1016/J.CEJ.2020.126600.
[31] K. Zhang, L. van Dyk, D. He, J. Deng, S. Liu, H. Zhao, Synthesis of zeolite from fly ash and its adsorption of phosphorus in wastewater, Green Process. Synth. 10 (2021) 349–360, https://doi.org/10.1515/GPS-2021-0032/ASSET/GRAPHIC/J_GPS-2021-0032_FIG_008.JPG.
[32] D. Mitrogiannis, M. Psychogiou, G. Manthos, K. Tsigkou, M. Kornaros, N. Koukouzas, D. Michailidis, D. Palles, E.I. Kamitsos, C. Mavrogonatos, I. Baziotis, Phosphorus and potassium recovery from anaerobically digested olive mill wastewater using modified zeolite, fly ash and zeolitic fly ash: a comparative study, J. Chem. Technol. Biotechnol. (2022), https://doi.org/10.1002/JCTB.7059.
[33] P. Kunecki, R. Panek, M. Wdowin, W. Franus, Synthesis of faujasite (FAU) and tschernichite (LTA) type zeolites as a potential direction of the development of lime Class C fly ash, Int. J. Miner. Process. 166 (2017) 69–78, https://doi.org/10.1016/J.MINPRO.2017.07.007.
[34] R. Panek, J. Madej, L. Bandura, G. Słowik, Recycling of waste solution after hydrothermal conversion of fly ash on a semi-technical scale for zeolite synthesis, Materials Vol. 14 (2021) 1413, https://doi.org/10.3390/MA14061413.
[35] M. Kragović, A. Daković, Ž. Sekulić, M. Trgo, M. Ugrina, J. Perić, G.D. Gatta, Removal of lead from aqueous solutions by using the natural and Fe(III)-modified zeolite, Appl. Surf. Sci. 258 (2012) 3667–3673, https://doi.org/10.1016/J.APSUSC.2011.12.002.
[36] H. Freundlich, Über die Adsorption in Lösungen, Z. Phys. Chem. 57U (1907) 385–470, https://doi.org/10.1515/ZPCH-1907-5723.
[37] I. Michalak, S. Baśladyńska, M. Mularczyk, K. Marycz, Investigation on the potential sorbents — aluminosilicate, microalga and grass hay as feed additives, Environ. Technol. Innov. 24 (2021), 101816, https://doi.org/10.1016/J.ETI.2021.101816.
[38] J. Mokrzycki, I. Michalak, P. Rutkowski, Biochars obtained from freshwater biomass—green macroalga and hornwort as Cr(III) ions sorbents, Biomass Convers. Biorefin. 11 (2021) 301–313, https://doi.org/10.1007/S13399-020-00649-6/TABLES/7.
[39] M. Heydari Moghaddam, R. Nabizadeh, M.H. Dehghani, B. Akbarpour, A. Azari, M. Yousefi, Performance investigation of zeolitic imidazolate framework – 8 (ZIF-8) in the removal of trichloroethylene from aqueous solutions, Microchem. J. 150 (2019), 104185, https://doi.org/10.1016/J.MICROC.2019.104185.
[40] ISO – ISO 11885:2007 – Water quality — Determination of Selected Elements by Inductively Coupled Plasma Optical Emission Spectrometry (ICP-OES), (n.d.). ⟨https://www.iso.org/standard/36250.html⟩, (Accessed 22 April 2022).
[41] S. Chen, J. Popovich, W. Zhang, C. Ganser, S.E. Haydel, D.K. Seo, Superior ion release properties and antibacterial efficacy of nanostructured zeolites ion-exchanged with zinc, copper, and iron, RSC Adv. 8 (2018) 37949–37957, https://doi.org/10.1039/C8RA06556J.
[42] G. Yao, J. Lei, W. Zhang, C. Yu, Z. Sun, S. Zheng, S. Komarneni, Antimicrobial activity of X zeolite exchanged with Cu 2+ and Zn 2+ on Escherichia coli and Staphylococcus aureus, Environ. Sci. Pollut. Res. 26 (2019) 2782–2793, https://doi.org/10.1007/S11356-018-3750-Z/FIGURES/14.
[43] F. Benaliouche, Y. Boucheffa, P. Ayrault, S. Mignard, P. Magnoux, NH3-TPD and FTIR spectroscopy of pyridine adsorption studies for characterization of Ag- and Cu-exchanged X zeolites, Microporous Mesoporous Mater. 111 (2008) 80–88, https://doi.org/10.1016/J.MICROMESO.2007.07.006.
[44] G. Sethia, R.S. Somani, H. Chand Bajaj, Adsorption of carbon monoxide, methane and nitrogen on alkaline earth metal ion exchanged zeolite-X: structure, cation position and adsorption relationship, RSC Adv. (2015), https://doi.org/10.1039/c4ra11511b.
[45] A. Nezamzadeh-Ejhieh, S. Hushmandrad, Solar photodecolorization of methylene blue by CuO/X zeolite as a heterogeneous catalyst, Appl. Catal. A Gen. 388 (2010) 149–159, https://doi.org/10.1016/J.APCATA.2010.08.042.
[46] L. Bandura, R. Panek, J. Madej, W. Franus, Synthesis of zeolite-carbon composites using high-carbon fly ash and their adsorption abilities towards petroleum substances, Fuel 283 (2021), 119173, https://doi.org/10.1016/J.FUEL.2020.119173.
[47] K.M. Kim, H.T. Oh, S.J. Lim, K. Ho, Y. Park, C.H. Lee, Adsorption equilibria of water vapor on zeolite 3A, Zeolite 13X, and dealuminated y zeolite, J. Chem. Eng. Data 61 (2016) 1547–1554, https://doi.org/10.1021/ACS.JCED.5B00927/ASSET/IMAGES/MEDIUM/JE-2015-00927U_0006.GIF.
[48] M. Thommes, K. Kaneko, A.v. Neimark, J.P. Olivier, F. Rodriguez-Reinoso, J. Rouquerol, K.S.W. Sing, Physisorption of gases, with special reference to the evaluation of surface area and pore size distribution (IUPAC technical report), Pure Appl. Chem. 87 (2015) 1051–1069, https://doi.org/10.1515/PAC-2014-1117/PDF.
[49] H. Golipour, B. Mokhtarani, M. Mafi, A. Moradi, H.R. Godini, Experimental measurement for adsorption of ethylene and ethane gases on copper-exchanged zeolites 13X and 5A, J. Chem. Eng. Data 65 (2020) 3920–3932, https://doi.org/10.1021/ACS.JCED.0C00251.
[50] S. Yurdakal, C. Garlisi, L. Özcan, M. Bellardita, G. Palmisano, (Photo)catalyst characterization techniques: adsorption isotherms and BET, SEM, FTIR, UV–Vis, photoluminescence, and electrochemical characterizations, Heterog. Photocatal. Relatsh. Heterog. Catal. Perspect. (2019) 87–152, https://doi.org/10.1016/B978-0-444-64015-4.00004-3.
[51] G.D. Gatta, P. Cappelletti, B. de' Gennaro, N. Rotiroti, A. Langella, New data on Cu-exchanged phillipsite: a multi-methodological study, Phys. Chem. Miner. 42 (2015) 723–733, https://doi.org/10.1007/S00269-015-0757-6/FIGURES/10.
[52] M. Zhang, X. Wang, Preparation of a gangue-based X-type zeolite molecular sieve as a multiphase fenton catalyst and its catalytic performance, ACS Omega 6 (2021) 18414–18425, https://doi.org/10.1021/ACSOMEGA.1C02469/ASSET/IMAGES/LARGE/AO1C02469_0012.JPEG.
[53] M.I. Binay, S.K. Kirdeciler, B. Akata, Development of antibacterial powder coatings using single and binary ion-exchanged zeolite A prepared from local kaolin, Appl. Clay Sci. 182 (2019), 105251, https://doi.org/10.1016/J.CLAY.2019.105251.
[54] N. Hamdi, E. Srasra, Removal of phosphate ions from aqueous solution using Tunisian clays minerals and synthetic zeolite, J. Environ. Sci. 24 (2012) 617–623, https://doi.org/10.1016/S1001-0742(11)60791-2.
[55] L.F. Capa-Cobos, X. Jaramillo-Fierro, S. González, Computational study of the adsorption of phosphates as wastewater pollutant molecules on faujasites, Processes Vol. 9 (2021) 1821, https://doi.org/10.3390/PR9101821.
[56] S. Senthilkumar, W. Zhong, M. Natarajan, C. Lu, B. Xu, X. Liu, A green approach for aerobic oxidation of benzylic alcohols catalysed by CuI–Y zeolite/TEMPO in ethanol without additional additives, New J. Chem. 45 (2021) 705–713, https://doi.org/10.1039/D0NJ03776A.
[57] L. Bandura, R. Panek, J. Madej, W. Franus, Synthesis of zeolite-carbon composites using high-carbon fly ash and their adsorption abilities towards petroleum substances, Fuel 283 (2021), 119173, https://doi.org/10.1016/J.FUEL.2020.119173.
[58] S. Hokkanen, E. Repo, L.J. Westholm, S. Lou, T. Sainio, M. Sillanpää, Adsorption of Ni2+, Cd2+, PO43− and NO3− from aqueous solutions by nanostructured microfibrillated cellulose modified with carbonated hydroxyapatite, Chem. Eng. J. 252 (2014) 64–74, https://doi.org/10.1016/J.CEJ.2014.04.101.
[59] Y. Guo, T. Li, Z. Chen, C. Bian, L. Pang, Efficient strategy to regenerate phosphorus-poisoned Cu-SSZ-13 catalysts for the NH3-SCR of NOx: the deactivation and promotion mechanism of phosphorus, ACS Catal. 11 (2021) 12963–12976, https://doi.org/10.1021/ACSCATAL.1C03752/SUPPL_FILE/CS1C03752_SI_001.PDF.
[60] Y. He, H. Lin, Y. Dong, B. Li, L. Wang, S. Chu, M. Luo, J. Liu, Zeolite supported Fe/Ni bimetallic nanoparticles for simultaneous removal of nitrate and phosphate: synergistic effect and mechanism, Chem. Eng. J. 347 (2018) 669–681, https://doi.org/10.1016/J.CEJ.2018.04.088.
[61] D. Mitrogiannis, M. Psychoyou, I. Baziotis, V.J. Inglezakis, N. Koukouzas, N. Tsoukalas, D. Palles, E. Kamitsos, G. Oikonomou, G. Markou, Removal of phosphate from aqueous solutions by adsorption onto Ca(OH)2 treated natural

clinoptilolite, Chem. Eng. J. 320 (2017) 510–522, https://doi.org/10.1016/J.CEJ.2017.03.063.
[62] M.S. Onyango, D. Kuchar, M. Kubota, H. Matsuda, Adsorptive removal of phosphate ions from aqueous solution using synthetic zeolite, Ind. Eng. Chem. Res. 46 (2007) 894–900, https://doi.org/10.1021/IE060742M.
[63] T.H. Pham, K.M. Lee, M.S. Kim, J. Seo, C. Lee, La-modified ZSM-5 zeolite beads for enhancement in removal and recovery of phosphate, Microporous Mesoporous Mater. 279 (2019) 37–44, https://doi.org/10.1016/J.MICROMESO.2018.12.017.
[64] N. Hamdi, E. Srasra, Removal of phosphate ions from aqueous solution using Tunisian clays minerals and synthetic zeolite, J. Environ. Sci. 24 (2012) 617–623, https://doi.org/10.1016/S1001-0742(11)60791-2.
[65] W. Shi, Y. Fu, W. Jiang, Y. Ye, J. Kang, D. Liu, Y. Ren, D. Li, C. Luo, Z. Xu, Enhanced phosphate removal by zeolite loaded with Mg–Al–La ternary (hydr)oxides from aqueous solutions: performance and mechanism, Chem. Eng. J. 357 (2019) 33–44, https://doi.org/10.1016/J.CEJ.2018.08.003.
[66] J.C. Bullen, S. Saleesongsom, K. Gallagher, D.J. Weiss, A revised pseudo-second-order kinetic model for adsorption, sensitive to changes in adsorbate and adsorbent concentrations, Langmuir 37 (2021) 3189–3201, https://doi.org/10.1021/ACS.LANGMUIR.1C00142/SUPPL_FILE/LA1C00142_SI_001.PDF.
[67] M. Andrunik, T. Bajda, Removal of pesticides from waters by adsorption: comparison between synthetic zeolites and mesoporous silica materials. A review, Materials 14 (2021), https://doi.org/10.3390/ma14133532.
[68] K.L. Tan, B.H. Hameed, Insight into the adsorption kinetics models for the removal of contaminants from aqueous solutions, J. Taiwan Inst. Chem. Eng. 74 (2017) 25–48, https://doi.org/10.1016/j.jtice.2017.01.024.
[69] E. Lorenc-Grabowska, P. Rutkowski, High adsorption capacity carbons from biomass and synthetic polymers for the removal of organic compounds from water, Water Air Soil Pollut. 225 (2014) 1–10, https://doi.org/10.1007/S11270-014-2082-Y/FIGURES/5.
[70] C. Ma, X. Zhang, K. Wen, R. Wang, R. Han, Facile synthesis of polyethyleneimine@Fe3O4 loaded with zirconium for enhanced phosphate adsorption: performance and adsorption mechanism, Korean J. Chem. Eng. 38 (2021) 135–143, https://doi.org/10.1007/S11814-020-0663-6.
[71] J.K. Kang, E.J. Seo, C.G. Lee, S.J. Park, Fe-loaded biochar obtained from food waste for enhanced phosphate adsorption and its adsorption mechanism study via spectroscopic and experimental approach, J. Environ. Chem. Eng. 9 (2021), 105751, https://doi.org/10.1016/J.JECE.2021.105751.
[72] J. López-Luna, L.E. Ramírez-Montes, S. Martinez-Vargas, A.I. Martínez, O. F. Mijangos-Ricardez, M. del, C.A. González-Chávez, R. Carrillo-González, F. A. Solís-Domínguez, M. del, C. Cuevas-Díaz, V. Vázquez-Hipólito, Linear and nonlinear kinetic and isotherm adsorption models for arsenic removal by manganese ferrite nanoparticles, SN Appl. Sci. 1 (2019) 1–19, https://doi.org/10.1007/S42452-019-0977-3/TABLES/7.
[73] H. Thagira Banu, P. Karthikeyan, S. Meenakshi, Lanthanum (III) encapsulated chitosan-montmorillonite composite for the adsorptive removal of phosphate ions from aqueous solution, Int. J. Biol. Macromol. 112 (2018) 284–293, https://doi.org/10.1016/J.IJBIOMAC.2018.01.138.
[74] C. Wan, S. Ding, C. Zhang, X. Tan, W. Zou, X. Liu, X. Yang, Simultaneous recovery of nitrogen and phosphorus from sludge fermentation liquid by zeolite adsorption: mechanism and application, Sep. Purif. Technol. 180 (2017) 1–12, https://doi.org/10.1016/J.SEPPUR.2017.02.031.
[75] S. Malamis, E. Katsou, A review on zinc and nickel adsorption on natural and modified zeolite, bentonite and vermiculite: examination of process parameters, kinetics and isotherms, J. Hazard. Mater. 252–253 (2013) 428–461, https://doi.org/10.1016/J.JHAZMAT.2013.03.024.
[76] Q. Xu, W. Li, L. Ma, D. Cao, G. Owens, Z. Chen, Simultaneous removal of ammonia and phosphate using green synthesized iron oxide nanoparticles dispersed onto zeolite, Sci. Total Environ. 703 (2020), 135002, https://doi.org/10.1016/J.SCITOTENV.2019.135002.
[77] M.A. Lewis, D.F. Fischer, L.J. Smith, Salt-occluded zeolites as an immobilization matrix for chloride waste salt, J. Am. Ceram. Soc. 76 (1993) 2826–2832, https://doi.org/10.1111/J.1151-2916.1993.TB04023.X.
[78] R. Jarosz, J. Szerement, K. Gondek, M. Mierzwa-Hersztek, The use of zeolites as an addition to fertilisers – a review, Catena 213 (2022), 106125, https://doi.org/10.1016/J.CATENA.2022.106125.
[79] J. Szerement, A. Szatanik-Kloc, R. Jarosz, T. Bajda, M. Mierzwa-Hersztek, Contemporary applications of natural and synthetic zeolites from fly ash in agriculture and environmental protection, J. Clean. Prod. 311 (2021), 127461, https://doi.org/10.1016/J.JCLEPRO.2021.127461.
[80] B. Bonetti, E.C. Waldow, G. Trapp, M.E. Hammercshmitt, S.F. Ferrarini, M.J.R. Pires, S.T. Estevam, Thiago, F.D. Aquino, Production of Zeolitic Materials in Pilot Scale Based on Coal Ash for Phosphate and Potassium Adsorption in Order to Obtain Fertilizer, (n.d.). ⟨https://doi.org/10.1007/s11356-020⟩.
[81] C. Ballabio, P. Panagos, E. Lugato, J.H. Huang, A. Orgiazzi, A. Jones, O. Fernández-Ugalde, P. Borrelli, L. Montanarella, Copper distribution in European topsoils: an assessment based on LUCAS soil survey, Sci. Total Environ. 636 (2018) 282–298, https://doi.org/10.1016/J.SCITOTENV.2018.04.268.
[82] L. Chen, Y. Shen, Q. Wang, X. Wang, Y. Wang, B. Li, S. Li, S. Zhang, W. Li, Phosphate on ceria with controlled active sites distribution for wide temperature NH3-SCR, J. Hazard. Mater. 427 (2022), 128148, https://doi.org/10.1016/J.JHAZMAT.2021.128148.
[83] Z. Chen, C. Fan, L. Pang, S. Ming, P. Liu, T. Li, The influence of phosphorus on the catalytic properties, durability, sulfur resistance and kinetics of Cu-SSZ-13 for NOx reduction by NH3-SCR, Appl. Catal. B Environ. 237 (2018) 116–127, https://doi.org/10.1016/J.APCATB.2018.05.075.